THE INVESTIGATION OF FIBRE REINFORCEMENT EFFECTS IN THERMOPLASTIC MATERIALS: INTERFACIAL BOND STRENGTH AND FIBRE END PARAMETER

C.C.Wang[1], J.L.Thomason[2] and F.R.Jones[1]

[1] *Department of Engineering Materials, University of Sheffield, Sheffield, S1 3JD, UK:*

[2] *Department of Mechanical Engineering, University of Strathclyde, Glasgow, G1 1XJ,U.K*

ABSTRACT

Microbond adhesion tests and photoelastic studies have been used to investigate the interfacial micro-mechanism of a glass fibre in a polyamide matrix. Furthermore, γ-aminopropyltriethoxysilane was used to modify the stress transfer efficiency at the interface. Experimental results show that the interfacial bond strength of silanized glass fibre is significantly increased. By examining the silanisation of the fibre-ends, it has been shown that "end-adhesion" should not be excluded from stress transfer models. Furthermore, the stress concentrations associated with non-silanized fractured fibre-ends is shown to lead to premature debonding.

1. INTRODUCTION

Short fibre reinforced thermoplastics (SFRT) are usually used for injection moulding. Transport of the polymer containing short glass fibres along the screw leads to the fracture of fibres under bending loads. This leads to distribution of fibre lengths in the moulding, which is less appreciated is that the fibres which fracture under a bending moment leave non-square fractured ends, as shown in Figure 1.

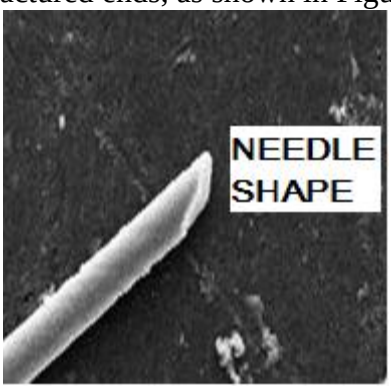

Figure 1 SEM picture of fractured needle shaped glass fibre-end after injection moulding

Previous studies by Curtis[1] and Sato[2] showed that the failure of short glass fibre reinforced composite was initiated by the debonding at fibre-ends. So we have sufficient reason to suspect that the non-square fractured fibre-ends initiate debonding and cause premature failure of the composite.

In this paper, the adhesive property of the silanized glass fibre unperturbed by the presence of a broken-end has been studied using the microbond test while the effect of a needle shaped fibre-end in the polyamide matrix has been studied by phase-stepping photoelasticity[3]. Furthermore, the role of a silane coupling agent on the stress transfer from the needle shaped fibre-ends has also been studied.

2. EXPERIMENTAL PROCEDURES

2.1 Fibres for microbond tests

Continuous water sized boron-free E-glass fibres were supplied by Owens Corning. "As received" water sized glass fibres were dried in a vacuum oven for 48 hour. Bundles were immersed in 1% γ-aminopropyltriethoxysilane (APS) (GE Speciality) aqueous solution at a pH of 10.6 for 15 minutes and then washed in deionized water at 50℃ for 24 h. The latter treatment was designed to remove physisorbed silane oligomers[4]. They were then dried at room temperature in a vacuum oven. These glass fibres are referred to as "silanized" glass fibres.

The mechanical properties of control fibres and silanized fibres were measured by single fibre tensile tests. Fibre strengths and Weibull Modules of these two types of glass fibre were shown in Table 1.

Table 1 Mechanical properties of single glass fibres used in the experiments

	Fibre strength (GPa)	Weibull Modulus
Control fibre	1.54±0.7	2.65
Silanized fibre	1.63±0.7	2.99

2.2 Fibres for photoelasticity studies

A long control fibre was cut by knife manually at an angle into several parts to obtain the needle shaped fibre-ends. These short glass fibres were then silanized using the procedure described in section 2.1 and some were used in photoelasticity. These silanized short fibres are referred to as "end-silanized" needle shaped glass fibres.

The remaining silanized short glass fibres were cut again to obtain the unsilanized surfaces at the top of the needle shaped fibre-ends. These short glass fibres were called "end-unsilanized" needle shaped glass fibres.

2.3 Polymer matrix

Amorphous polyamide (Grilamid TR55 supplied by EMS-Grivory) was chosen as the matrix to avoid problems associated with different degrees of crystallinity. Dog-bone shape polyamide specimens were prepared from the PA granules by injection moulding. The mechanical properties of TR55 amorphous polyamide material are shown below in Table 2.

Table 2 mechanical properties of amorphous polyamide

	Extension rate	Tensile strength at yield (MPa)	Strain at yield (%)
polyamide dog-bone specimen	0.13mm/min	62.7±0.7	11.6±0.1

2.4 Microbond test specimen preparation

Gaur[5] used very thin thermoplastic films to form a droplet on a single fibre. Later Yun[6] used single filaments, which were obtained from melted polyamide granule, to form a droplet on a single fibre. The sample preparation method described in this paper is similar to the approach of Yun[6].

A single amorphous polyamide granule was placed onto a hot plate and melted at 250℃. A thin single polyamide filament (diameter≈120 μm) was drawn from the melted granule and looped on a single glass fibre attached to a support frame, as shown in Figure 2. The glass fibre was lifted up as soon as the bottom of polyamide filament was remelted. Therefore only a very small amount of polyamide resin was

looped over the single glass fibre.

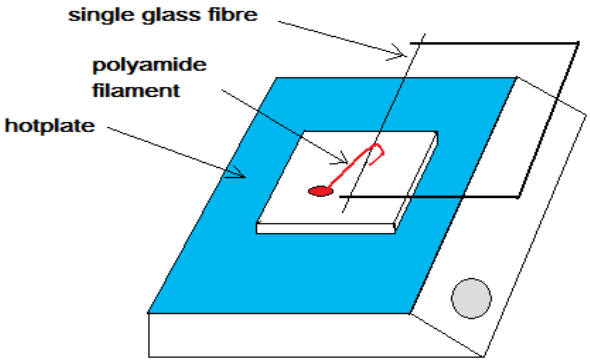

Figure 2 Schematic diagram of microbond test sample preparation

The polyamide filament was remelted in a furnace by heating from 300℃ to 350℃ for 30±1 seconds to form a micro-droplet (diameter range from 80μm~130μm). After the microbond specimen was cooled to room temperature. A 1cm^2 size square tab was attached on one end of the specimen, as shown in Figure 3. Each specimen was stored in a petri-dish for further testing.

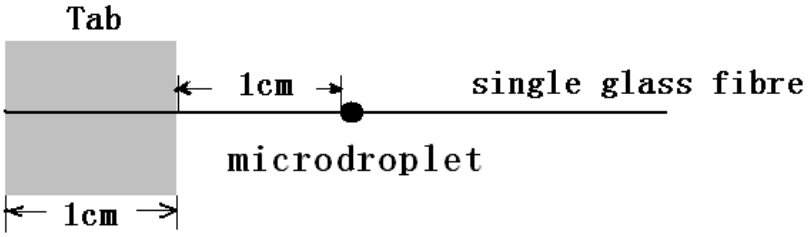

Figure 3 Schematic diagram of the microbond test specimen

The length of fibre embedded in the micro-droplet, the dimension of micro-droplet and the single fibre diameter for each specimen were recorded digitally using a microscope equipped image analyzing software.

2.5 Microbond test

The single fibre microbond test was performed using a tensile tester (Hounsfield universal tester, Tinius Olsen Ltd, U.K.) to debond the polymer micro-droplet from the fibre. A microvice was mounted onto a micro-droplet, as shown in Figure 4. A crosshead speed of 0.2 mm/min was used for each measurement. The force-displacement curve was measured with a 0~10 N range load cell and recorded by computer. Each microbond specimen was examined after testing to ensure that the micro-droplet had debonded from the single glass fibre surface.

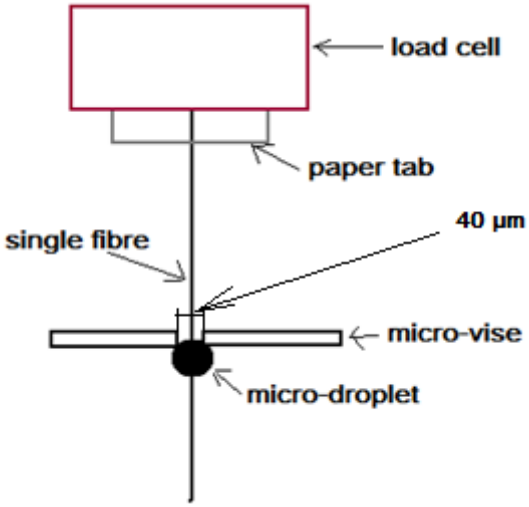

Figure 4 Schematic diagram of the microbond test

In the microbond test, more than 20 effective samples were tested for one group of specimens. Equation 1 was used to calculate the average interfacial shear stress (IFSS) values during microbond tests.

$$\tau = \frac{F}{\pi D l} \quad (1)$$

where F is the pull-out force from the microbond test. D is the fiber diameter and l is the embedded length of fibre in the micro-droplet

2.6 Sample preparation for photoelasticity test

In order to embed a short glass fibre into a dog-bone shaped polyamide specimen, a deep nick was cut into the middle of the specimen surface to form a thin "pocket". Then a short glass fibre (length≈10 µm) was placed in the pocket (Figure 5) and the entire dog-bone shape sample was heated on a hotplate in a female mould at 213℃. A dog-bone shape male mould was placed on the top of polyamide specimen to provide a constant pressure. Specimen was heated for 20 minutes to ensure that the embedded glass fibre was fully melted by the polyamide. After that, the specimen was removed from the mould and cooled down to room temperature. The specimens were stored under vacuum at room temperature to avoid moisture absorption.

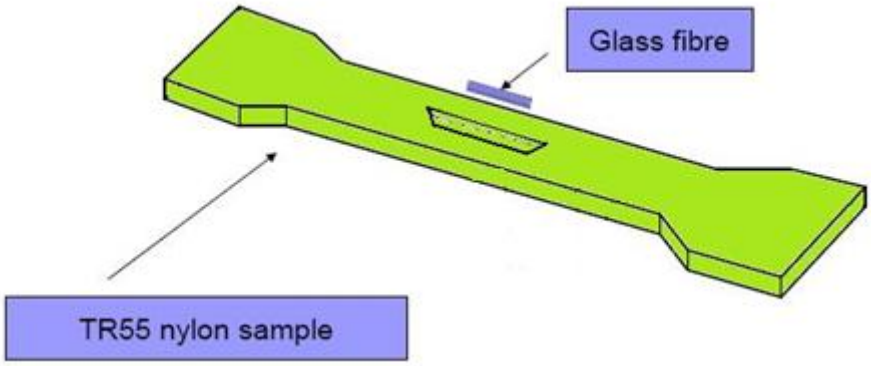

Figure 5 Schematic diagram of the method of embedding a short glass fibre into a polyamide specimen

2.7 Photoelasticity experiment

A phase-stepping automated photoelasticity equipment was mounted on a micro-tensile test machine (Micromaterials Ltd, Wrexham, U.K.) to capture the images during the test. This equipment has four CCD cameras for collecting the photoelasticity images simultaneously at four phase angles. Then 256×256 pixel images were transferred to a computer so that phase-stepping algorithms could be implemented.

The isoclinic angle θ and relevant retardation δ can be calculated by the equations 2 and 3 [3].

$$\theta = \frac{1}{2} tan^{-1} \frac{i_1 - i_3}{i_2 + i_3 - 2i_1} \tag{2}$$

$$\delta = tan^{-1} \frac{i_2 - i_3}{sin 2\theta (i_2 + i_3 - 2i_4)} \tag{3}$$

where i_1 to i_4 are the light intensities observed by the four CCD cameras. After the Retardation value was obtained, it can be algorithmed to the isochromatic value using the unwrapping procedure described by Patterson[3].

In photoelasticity, the difference between the principle stresses in a two-dimensional model can be related to the isochromatic fringe order by equation 4[7]. At the fibre-matrix interface, the principle stress difference $(\sigma_1 - \sigma_2)$ can be thought of as the maximum shear stress so that the shear stress profiles at fibre/matrix interface can be obtained.

$$\frac{\tau_{max}}{2} = \frac{(\sigma_1 - \sigma_2)}{2} = \frac{fN}{t} \tag{4}$$

where f is the photoelasticity constant, N is the fringe order and t is the thickness of specimen.

If a small-diameter inclusion was embedded into the relatively thick specimen, the observed principle stress difference varies with the thickness of the specimen. A correction of the maximum shear stress values around single fibre can be calculated according to equations 5[8] and 6 [9].

$$\tau_{cmax} = \frac{1}{2}\left\{ \frac{t(\sigma_0 - \sigma_n)(r_1 - r_0)}{2\left\{ r_1\alpha - 0.5\left[r_1\alpha + (r_0 + y)2\log\left(\frac{\alpha + r_1}{r_0 + y} \right) \right] \right\}} + \sigma_n \right\} \tag{5}$$

where $\alpha = \left[r_1^{\,2} - (y + r_0)^2 \right]^{1/2}$

σ_0 =observed principal stress difference

σ_n =applied nominal matrix stress

r_1 =boundary of the fringe order

r_0 =fibre diameter

y=start point of the fringe order

t=the thickness of the sample

$$\tau_i = \tau_{cmax} \, sin2\theta \tag{6}$$

3. RESULTS

3.1 Microbond adhesion strength

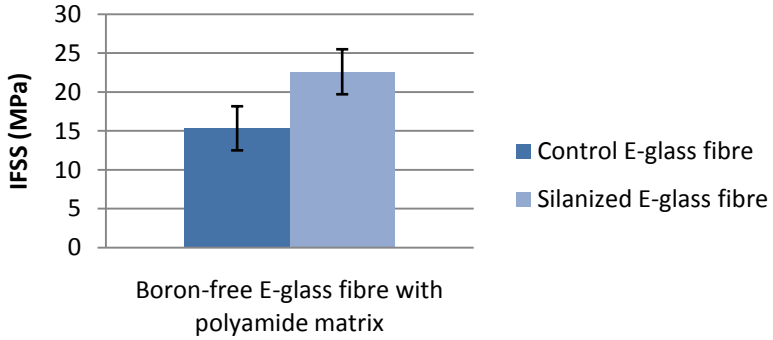

Figure 6 Comparison of interfacial shear strengths for unsilanized and silanized E-glass fibres in the amorphous polyamide matrix

As a prelude to the photoelasticity tests for these silanized needle shaped fibre-ends, the microbond test was used to predict the effect of the silane coupling agent on boron-free E-glass fibre/polyamide composite. As shown in Figure 6, use of the silane coupling agent on E-glass fibre improved the interfacial shear strength from 15 MPa to 23 MPa. This indicates that adhesion between glass fibre and polyamide matrix was significantly increased by the silane coupling agent.

3.2 Photoelasticity study

The birefringent patterns around the needle shaped glass fibre-ends in the polyamide matrix were studied using the 2-dimensional phase-stepping photoelasticity instrument. For the needle shaped glass fibres (average length: 9.01±0.5 mm), the birefringent patterns were observed around the fibre-end at the applied matrix stress range of 19~20MPa (equivalent applied strain values 1.1~1.2%). Phase-stepping photoelastic images were then captured at increasing intervals of applied uniaxial stresses on matrix.

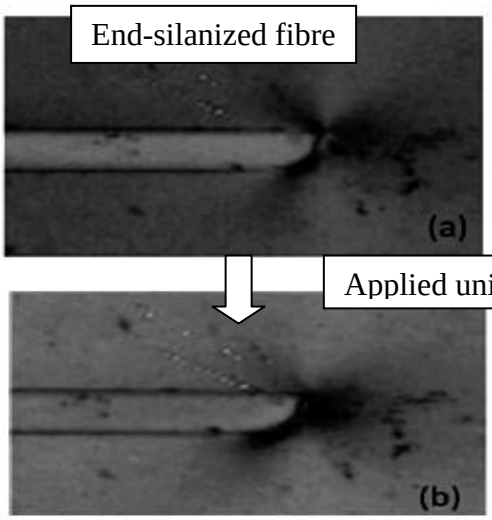

Figure 7 Birefringent patterns in polyamide matrix around end-silanized needle shaped fibre-end at the applied matrix stress of (a) 19 MPa (b) 23 MPa

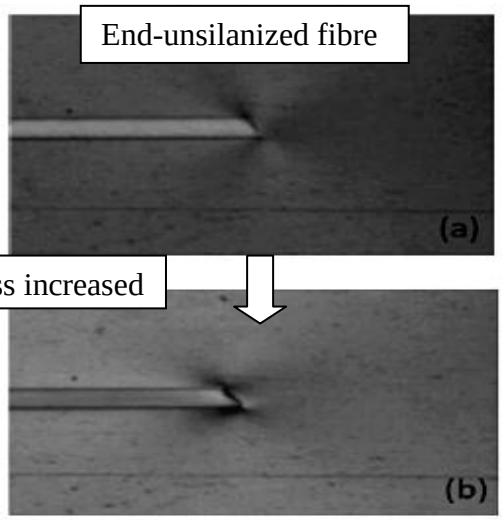

Figure 8 Birefringent patterns in polyamide matrix around end-unsilanized needle shaped fibre-end at the applied matrix stress of (a) 20 MPa (b) 24 MPa

Figure 7(a) shows the birefringent patterns appeared around the end of the end-silanized fibre at applied matrix stress of 19MPa, which indicated a stress concentration at the interface associated with the fibre-end. The birefringent pattern at the upper side of the interface disappeared when the uniaxial tensile stress on the matrix was increased from 19 MPa to 23 MPa, as shown in Figure 7(b). This shows that debonding was initiated at the end-silanized needle shaped fibre end.
In contrast, Figure 8(a) shows that the birefringent zone appeared at the interface of the end-unsilanized needle shaped fibre-end when the specimen was loaded to 20 MPa. This indicated the debonding occurred at the unsilanized fibre end. Further loading (from 20 MPa to 24 MPa) changed the shape of the birefringent pattern, as shown in Figure 8(b), but it was still the indication of a poorly bonded fibre-end.

4. DISCUSSION

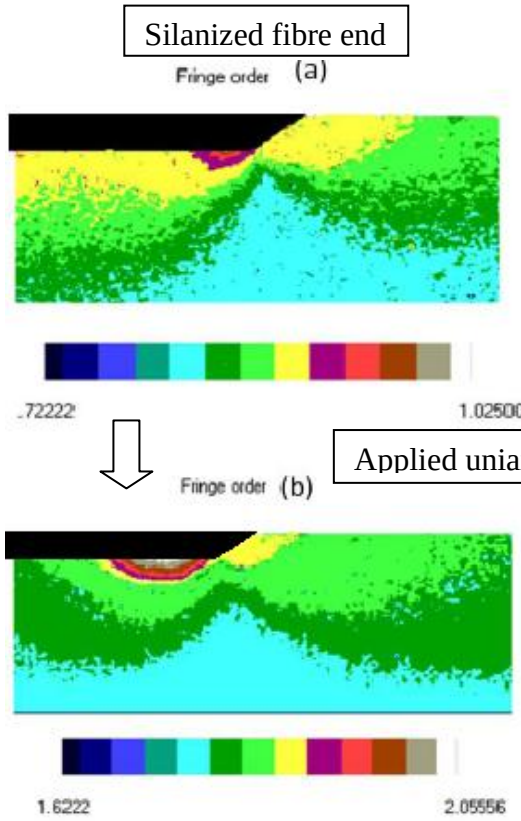

Figure 9 Contours maps of fringe order in polyamide matrix around end-silanized needle shaped fibre-end at the applied matrix stress of (a) 19 MPa (b) 23 MPa

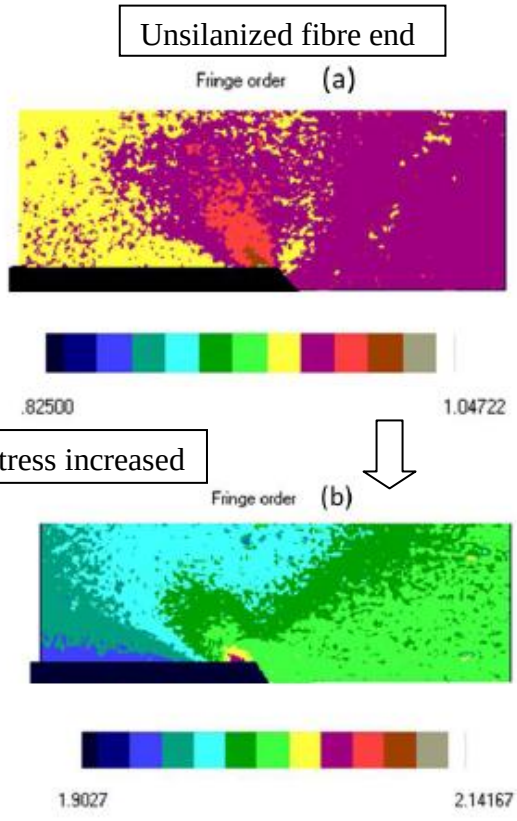

Figure 10 Contours maps of fringe order in polyamide matrix around end-unsilanized needle shaped fibre-end at the applied matrix stress of (a) 20 MPa (b) 24 MPa

A fringe order analysis of the combined birefringent patterns of the 4 phase-stepped photoelasticity images has been carried out. The contours maps of the fringe order around the needle shaped fibre-ends in the polyamide matrix are shown in Figure 9 and Figure 10. The fringe order zone at the "shorter" fibre length has been examined in detail.
From Figures 9, it is clear that stress transfer occurs along the fibre from the end. However, in the absence of the "silane" coating on the fibre end, which was shown in

Figure 10, the stress concentration associated with the "corner" of the fibre dominates the fringe order distribution. This stress concentration modifies the stress transfer function significantly at the interface. The effect is quantified by calculating the shear stress profiles, which is shown in the following paragraph.

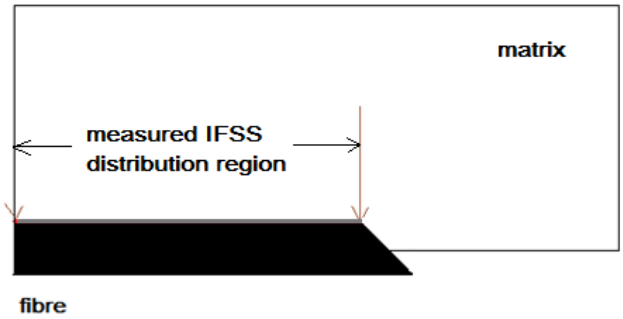

Figure 11 Schematic diagram of the "shorter" side of the fibre interface used for the analysis of the interfacial shear stress profile

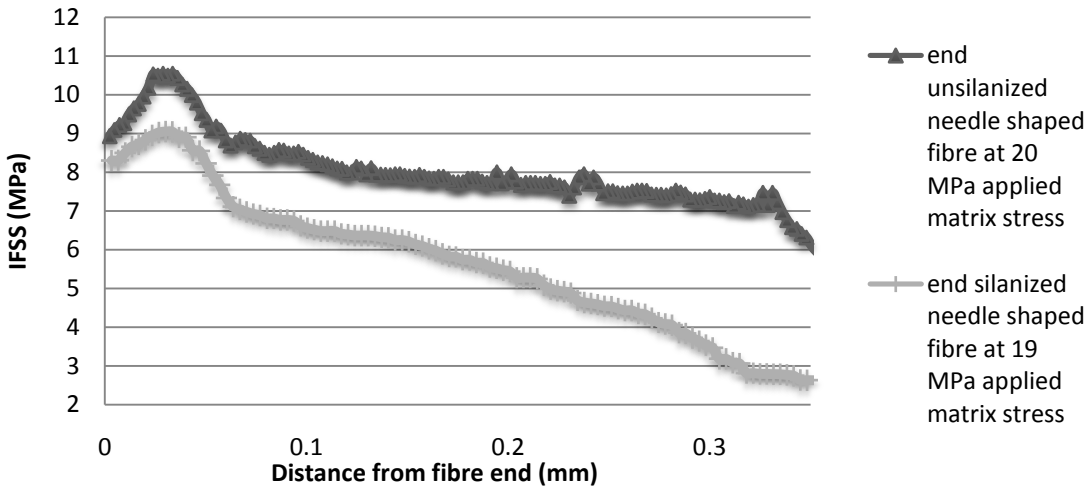

Figure 12 Profiles of IFSS for (a) end-unsilanized needle shaped fibre-end at 20 MPa (b) end-silanized needle shaped fibre-end at 19 MPa with distance from fibre ends

Figure 11 shows the interface region of the needle shaped fibre-end used for the calculation of IFSS from photoelasticity images. Figure 12 shows the IFSS profiles along the fibre from the end for the end-unsilanized and end-silanized needle shaped fibre interfaces at a similar applied matrix stresses (19~20 MPa). The maximum IFSS value for the end-silanized needle shaped fibre was approximately 9 MPa, which is lower than the value for end-unsilanized fibre, (≈11MPa).Figure 7 and 12 inferred that the bonded interface on the needle shape fibre end surface still transfer the stress from the matrix so that the shear stress values at the interface along the fibre was reduced.

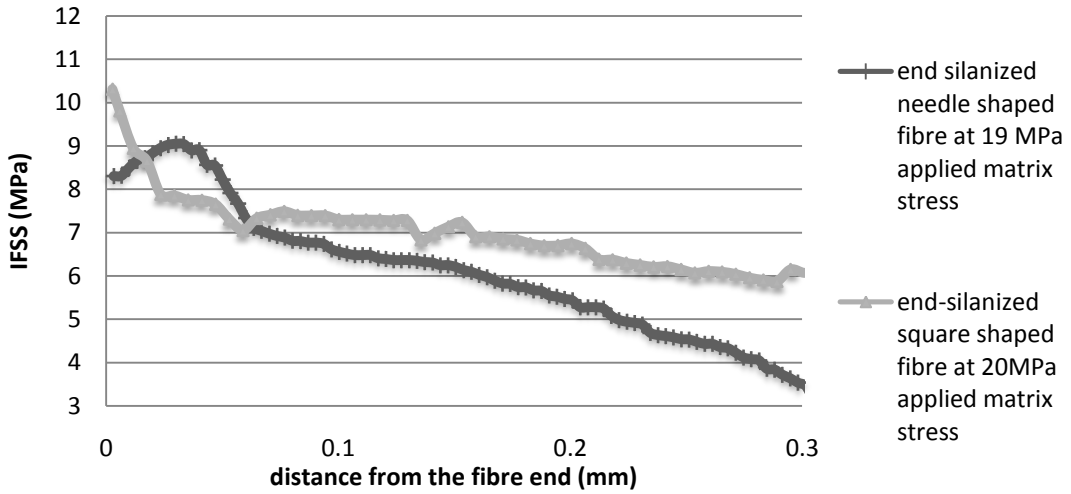

Figure 13 Profiles of IFSS for (a) end-silanized needle shaped fibre at 19 MPa (b) end-silanized square shaped fibre at 20 MPa with distance from fibre ends

In Figure 13, profile of IFSS at square shaped end-silanized fibre interface was used as a control. This can be contrasted with the data from the end-silanized needle shaped fibre at a similar applied matrix stress. It can be seen that the maximum IFSS for end bonded square shaped fibre (10.6 MPa) was higher than the value for end bonded needle shape fibre end (9 MPa). In addition, compared to the needle shaped fibre, the profile of IFSS for square shaped fibre indicated that the maximum interfacial shear stress appeared at the fibre end.

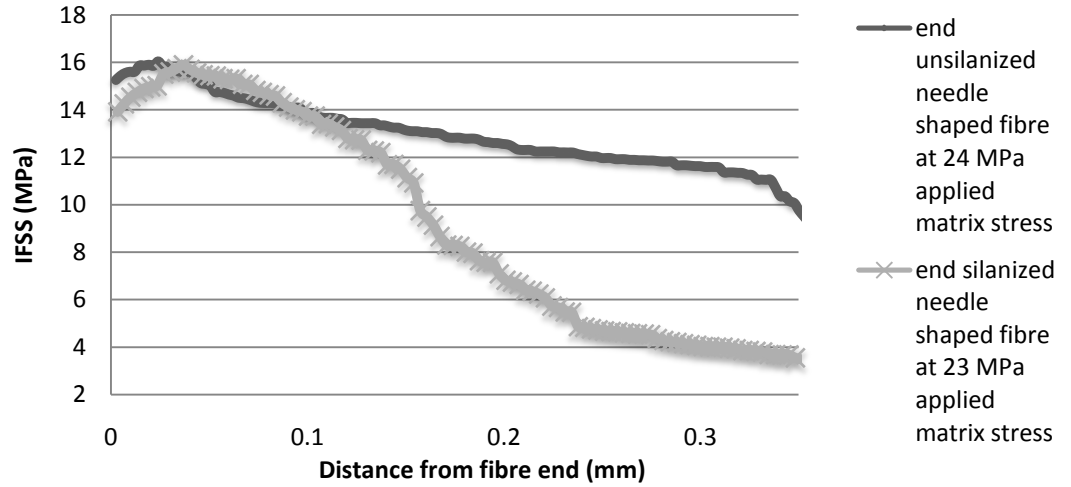

Figure 14 Profiles of IFSS for (a) end-unsilanized fibre end at 24 MPa (b) end-silanized fibre end at 23 MPa with distance from the fibre ends

When the applied matrix stress was increased by 4MPa, the silanized needle shaped fibre-end debonding from the matrix initiated. The debonding caused more stress transferred from the fibre end to the fibre/matrix interface so that the interfacial shear stress values along the fibre significantly increased. From Figure 14, it can be seen that the maximum IFSS value for the silanized fibre-end (16MPa) became equal to the value for the unsilanized fibre-end.

5. CONCLUSIONS

A thermoplastic microbond and photoelasticity techniques have been developed to investigate the micromechanics of the interfaces for silanized and unsilanized needle

shape fibre ends in a polyamide matrix. The results on microbond tests show that the silane coupling agent significantly improves the interfacial adhesion level between the boron-free E-glass fibre and polyamide matrix. Photoelastic analysis on end-silanized needle shaped fibre-end shows that the silane coupling agent on the end of fibre can effectively stop the debonding propagation and disperse the shear stress concentration at the interface in polyamide matrix.

6. ACKNOWLEDGEMENTS

The project is funded by EPSRC and European Owens Corning. We acknowledge the Owens Corning and EMS-Grivory for supplying E-glass fibres and polyamide granules. We thank Dr. F.M.Zhao and Prof. E.A.Patterson for introducing the phase-stepping photoelastic technique.

REFERENCES

1. Curtis, P.T., Bader, M.G. and Bailey,J.E. "The stiffness and strength of a polyamide thermoplastic reinforced with glass and carbon fibres", Journal of Materials Science, 1978;13: 377-390.
2. Sato, N., Kurauchi, T., Sato, S. and Kamigaito, O. "Microfailure behaviour of randomly dispersed short fibre reinforced thermoplastic composites obtained by direct SEM observation", Journal of Materials Science, 1991;26: 3891-3898.
3. Patterson, E.A. and Wang, Z.F. "Simultaneous observation of phase-stepped images for automated photoelasticity", Journal of Strain Analysis, 1998;33:. 1~15.
4. Wang, D., Jones, F.R. and Denison, P. "Surface analytical study of the interaction between γ-amino propyl triethoxysilane and E-glass surface", Journal of Materials Science, 1992;27: 36-48.
5. Gaur, U. "Measuring fibre/matrix adhesion in thermoplastic composites. Plastic Engineering", 1989: 43.
6. Yun, S.H., Cho, D., Kim, J., Lim, S., Lee, G., Park, M. and Lee, S. "Effect of silane coupling agents with different organo-functional groups on the interfacial shear strength of glass fiber-Nylon 6 composites". Journal of Materials Science Letters, 2003;22: 1591-1594.
7. Dally, J.W. and Riley,W.F. Experimental Stress Analysis. 1985, New York: Mcgraw-Hill.
8. Schuster, D.M. and Scala,E. "The Mechanical Interaction of Sapphire Whiskers with a Birefringent Matrix". Transactions of the Metallurgical Society of A.I.M.E, 1964;230: 1635~1640.
9. Fiedler, B. and Schulte,K. "Photo-elastic analysis of fibre-reinforced model composite materials". Composites Science and Technology, 1997;57: 859-867.